journal

J. Am. Ceram. Soc., 84 [5] 1010–16 (2001)

Influence of Dopant Concentration on Creep Properties of Nd_2O_3-Doped Alumina

Chong-Min Wang,* Junghyun Cho,* Helen M. Chan,* Martin P. Harmer,* and Jeffrey M. Rickman

Materials Research Center, Lehigh University, Bethlehem, Pennsylvania 18015

The microstructural features and tensile creep behavior of Al_2O_3 doped with Nd_2O_3 at levels ranging from 100 to 1000 ppm (Nd:Al atomic ratio) were systematically investigated. Compositional mapping, using both high-resolution scanning transmission electron microscopy and secondary ion mass spectroscopy revealed that, for all of the compositions studied, the Nd^{3+} ions were strongly segregated to the Al_2O_3 grain boundaries. Microstructural observations revealed that the solubility of Nd_2O_3 was between 100 and 350 ppm. Tensile creep tests were conducted over a range of temperatures (1200°–1350°C) and stresses (20–75 MPa). Both the stress and grain-size exponents were analyzed. In selected experiments, controlled grain-growth anneals were used to enable creep testing of samples of the same average grain size but different neodymium concentrations. Independent of dopant level, the neodymium additions decreased the creep rate by 2–3 orders of magnitude, compared with that of undoped Al_2O_3. The value of the apparent creep activation energy increased with increased dopant concentration and then saturated at dopant levels exceeding the solubility limit. Overall, the results of the present study were consistent with a creep-inhibition mechanism whereby oversized segregant ions reduce grain-boundary diffusivity by a site-blocking mechanism.

I. Introduction

In recent years, a series of studies has established the beneficial role of rare-earth-dopant ions on the creep behavior of Al_2O_3.[1–7] Thus, work by Lartigue *et al.*[1] and Robertson *et al.*[8] showed reductions in the creep rate of MgO-doped Al_2O_3, with the addition of yttrium, by factors of 5 and 15, respectively. The study of Cho *et al.*[4] demonstrated a more dramatic effect, whereby doping with yttrium or lanthanum improved the steady-state strain rate by 2–3 orders of magnitude (versus that of undoped Al_2O_3). In related work, Wakai *et al.*[9,10] observed that the addition of zirconium to Al_2O_3 (at levels both above and below the solubility limit) reduced the creep rate by a factor of 15.

More recently, Li *et al.* [7] reported the additional benefit that can derive from codoping with ions of disparate sizes. These workers showed that the enhancement in creep resistance for Nd/Zr codoped Al_2O_3 was greater than that achieved by doping with either neodymium or zirconium alone. The study of Li *et al.* also highlighted the influence of ionic size on the creep rate; thus, doping with Sc^{3+} (0.74 Å) or Zr^{4+} (0.72 Å), although still beneficial, was markedly less effective than doping with either La^{3+} (1.03 Å) or Y^{3+} (0.90 Å). Although previous work has suggested that the creep inhibition is primarily a solid-solution effect,[7,11] the influence of dopant concentration on creep behavior has not been systematically studied. Therefore, the objective of the present study was to address this issue, with regard to neodymium doping. In particular, it was hoped that any changes in behavior for the different solute levels would lend further insight to the creep mechanism.

II. Experimental Procedure

(1) Sample Preparation

The starting materials were ultra-pure α-Al_2O_3 powder (AKP-53, 99.995%, mean particle size 0.35 μm and specific surface area 12.7 m^2/g, Sumitomo Chemical America, Inc., New York, NY) and semiconductor-grade neodymium nitrate. Al_2O_3 samples with the following nominal Nd_2O_3 dopant levels were prepared: 100, 350, and 1000 ppm (Nd:Al atomic ratio). Details of the powder-processing and doping procedures are described elsewhere.[4,7] Dense billets (>99.5%) were obtained by hot-pressing the samples in a graphite die 76.2 μm in diameter, at 50 MPa for 30 min, in vacuum. The hot-pressing temperatures (which were tailored to achieve microstructures with comparable average grain sizes for the different compositions) were as follows: pure Al_2O_3, 1350°C; 100 ppm Al_2O_3, 1425°C; 350 and 1000 ppm neodymium, 1450°C.

(2) Creep Testing

Dog-bone-shaped tensile samples were machined from the hot-pressed billets, according to specifications described by French and Wiederhorn.[12] The sample gauge lengths were defined by two SiC flags attached to each sample and measured, using a laser extensometer (Beta LaserMike, Inc., Dayton, OH), to an accuracy of 1 μm. For each sample, possible flag slippage was monitored by measuring the projected flag thickness both before and after the creep test. If the change in projected flag thickness was >20 μm, the creep data were disregarded.

Previous work[4] showed that preannealing the creep samples under a slight load (5 MPa) significantly decreased the extent of primary creep. The microstructure was examined both before and after the preannealing treatment, and no change in grain size was detected. Therefore, before creep testing, all of the present samples were annealed at 1250°C for 24 h, under an applied stress of 5 MPa. Tensile creep tests were performed in air, whereby the sample was subjected to a constant load, using either a lever arm or a hydraulic testing machine (Applied Test Systems, Butler, PA). Testing was conducted in the temperature range 1200°–1350°C, with applied stresses ranging from 20 to 75 MPa. Three types of creep tests were performed: (i) a standard stress-rupture test, at 1275°C and 50 MPa; (ii) a temperature-step test, in which the stress was nominally kept constant, but the temperature was altered periodically; and (iii) a stress-step test, in which the temperature was held constant, but the stress was varied. The latter two types of tests enabled the measurement of the strain rate, under a given set of test conditions, two to three times per sample. For the range of stress and temperatures studied, no dependence of the steady-state strain rate on strain history was observed.

R. Raj—contributing editor

Manuscript No. 188999. Received October 22, 1999; approved October 12, 2000.
Supported by the U.S. Air Force Office of Scientific Research, under Grant No. F49620–98-1–0117.
*Member, American Ceramic Society.

The values of the stress exponent (n) and inverse grain-size exponent (p), as defined by the following constitutive equation, were also evaluated.

$$\dot{\varepsilon} = A\left(\frac{\sigma^n}{d^p}\right) \exp\left(-\frac{Q'}{RT}\right) \quad (1)$$

Here, $\dot{\varepsilon}$ is the strain rate, d the grain size, σ the applied stress, A a constant of proportionality determined by the slowest diffusive species along the fastest diffusion path, Q the activation energy, R the gas constant, and T the absolute temperature. To obtain n, stress-step testing was used to evaluate the steady-state strain rate at different stresses (at constant temperature and grain size). To evaluate p, the as-hot-pressed materials were annealed at 1450° and 1500°C for different times, to obtain a range of grain sizes for each composition; the samples were then tested at 1275°C, under a constant tensile loading of 50 MPa, until rupture.

Two distinct approaches were adopted to assess the dependence of creep resistance on the grain-boundary dopant concentration. In the first case, samples of the different dopant compositions were annealed to the same average grain size (2.4 ± 0.2 μm), and stress-rupture tests were conducted at 1275°C, under an applied stress of 50 MPa. In the second case, the creep behavior of samples with different grain sizes and dopant levels was normalized to the same grain size, using an experimentally determined value of p.

(3) Microstructure Analysis and Compositional Mapping

The microstructures of samples both before and after creep testing were evaluated by polishing each sample to a 1 μm diamond finish and thermally etching at 1400°C for 1 h. Grain size was determined from scanning electron micrographs, using the linear intercept method. The distribution of the neodymium dopant ions was characterized by both imaging secondary ion mass spectrometry (SIMS) (conducted at the University of Chicago) and analytical electron microscopy (AEM). Details of the SIMS procedure are given elsewhere.[6] In the case of the AEM, thin foils of both as-hot-pressed and deformed materials were prepared by standard techniques, including ultrasonic cutting, thinning, and dimpling, to a foil thickness of 120 μm, followed by ion-beam milling to perforation. A thin layer of carbon was evaporated on the sample to eliminate charging. Compositional mapping of the dopant distribution was conducted on a dedicated scanning transmission electron microscope (STEM; Model 603, VG Microscopes, West Sussex, U.K.) operating at 300 keV, fitted with a windowless Si(Li) detector (Link Systems, Boston, MA). The probe size was of the order of 0.6 nm, yielding an areal resolution of ~1 nm^2.

III. Results

(1) Microstructure and Neodymium Segregation Behavior

Scanning electron micrographs of the polished and thermally etched surfaces of the as-hot-pressed samples are shown in Fig. 1.

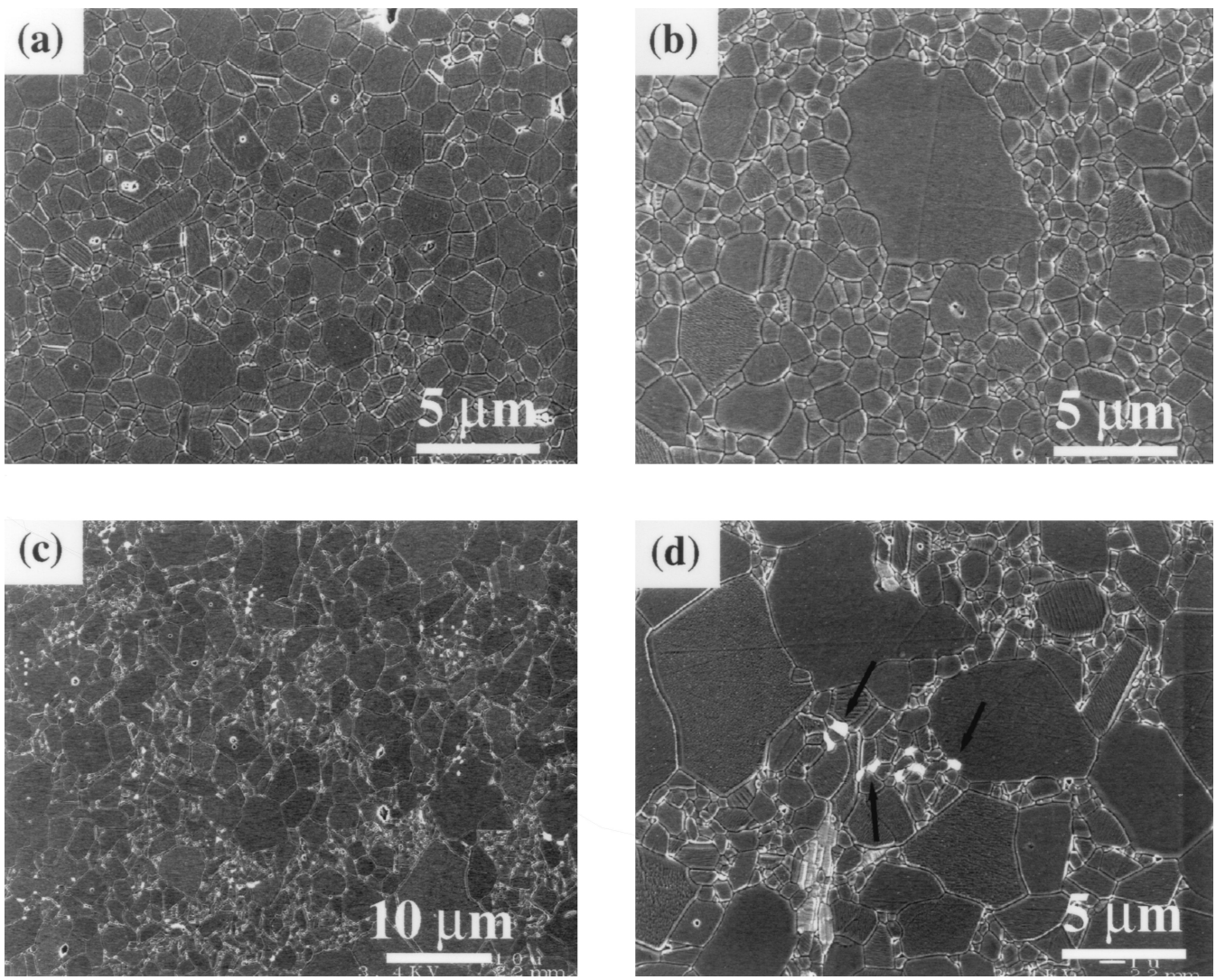

Fig. 1. SEM micrographs showing the microstructures of the as-hot-pressed neodymium-doped aluminas: (a) 100, (b) 350, and (c) and (d) 1000 ppm (arrows indicate secondary-phase precipitates).

The grains of the 100 ppm doped material are equiaxed and exhibit a uniform size distribution, with an average grain size of ~1.5 μm (see Fig. 1 (a)). No second-phase precipitates were observed for this composition, either by scanning electron microscopy (SEM) or transmission electron microscopy (TEM). In contrast, neodymium-rich precipitates occasionally were observed at grain-boundary triple points in the 350 ppm neodymium-doped material. The grain structure also differed from the 100 ppm sample in that, interspersed in a background of fine ($d \approx 1.5$ μm) grains, were larger grains up to 10 μm in size (Fig. 1(b)). From the micrographs, it was estimated that the large abnormal grains made up ~3% (by volume) of the structure. The microstructure of the 1000 ppm doped material was the most inhomogeneous of the three compositions, exhibiting essentially a bimodal grain-size distribution, with clusters of fine- and coarse-grain-size regions. For this dopant level, numerous second-phase particles were visible, preferentially situated in the fine-grain-size regions (Figs. 1(c) and (d)).

Figure 2 shows SIMS maps of the neodymium distribution in the as-hot-pressed materials; the regions of brighter contrast correspond to a locally higher neodymium content. As shown in the maps, Nd^{3+} ions are strongly segregated to the grain boundaries. The marked segregation behavior, even at the 100 ppm dopant level, confirms the very low solubility of neodymium in the Al_2O_3 lattice.

TEM observation revealed that the microstructures of the crept materials were characterized by an occasional dislocation array and two distinct forms of cavity (Fig. 3 and Fig. 4). The first type of cavity consisted of intragranular pores, which often exhibited a faceted morphology (Figs. 3(a) and 4(a)). Comparison of the deformed and undeformed materials established that these intragranular pores were residual pores following densification. The other type of cavity tended to be triangular in shape and located primarily at grain-boundary triple junctions (Fig. 3(b)). For the 1000 ppm sample (which essentially exhibited a bimodal grain size), these cavities occurred preferentially at the interface between large abnormal grains and surrounding small grains.

Similar cavitation features also have been reported by Chokshi and Porter[13] in crept Al_2O_3 codoped with 250 ppm MgO and 250 ppm ZrO_2 and possessing a bimodal grain-size distribution. A theoretical explanation for this cavitation phenomenon has been developed by Dalgleish *et al.*[14] and Chokshi and Porter,[13] predicting a localized doubling of the effective stress at the coarse-grained clusters, therefore inducing cavitations in these regions. Dedicated STEM analysis of dopant distribution confirmed the SIMS findings, namely that neodymium is mainly segregated to grain boundaries (see Fig. 5). However, no evidence was obtained for the segregation of neodymium ions to dislocation cores.

(2) Creep Behavior

The stress-rupture tests revealed that, independent of dopant level, the general features of the creep-deformation behavior were similar, with well-defined primary, steady-state, and tertiary deformation stages. Typically, the creep-rupture strain was ~15% for the 100 ppm doped material, ~8% for the 350 ppm doped material, and ~3% for the 1000 ppm doped material.

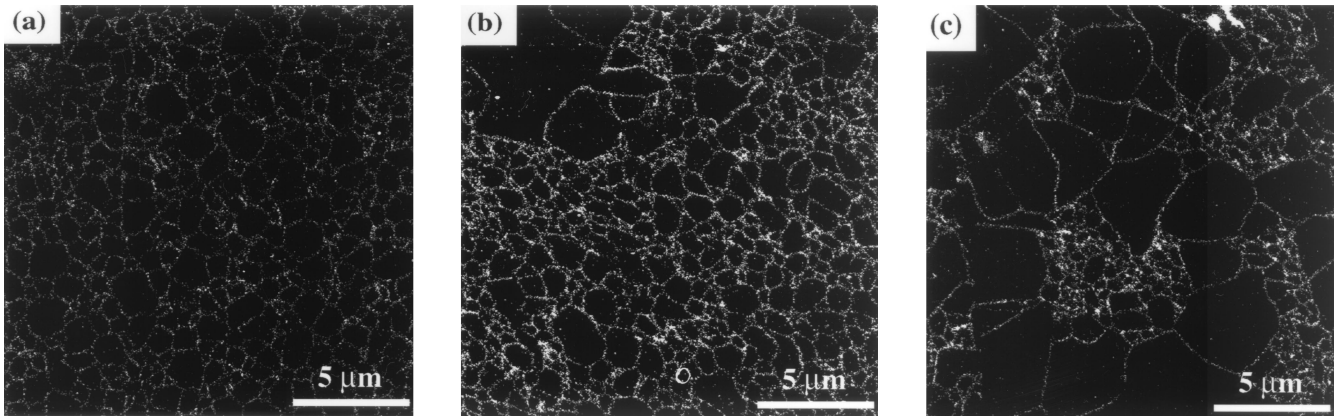

Fig. 2. SIMS map showing the neodymium distribution in the as-hot-pressed materials: (a) 100, (b) 350, and (c) 1000 ppm.

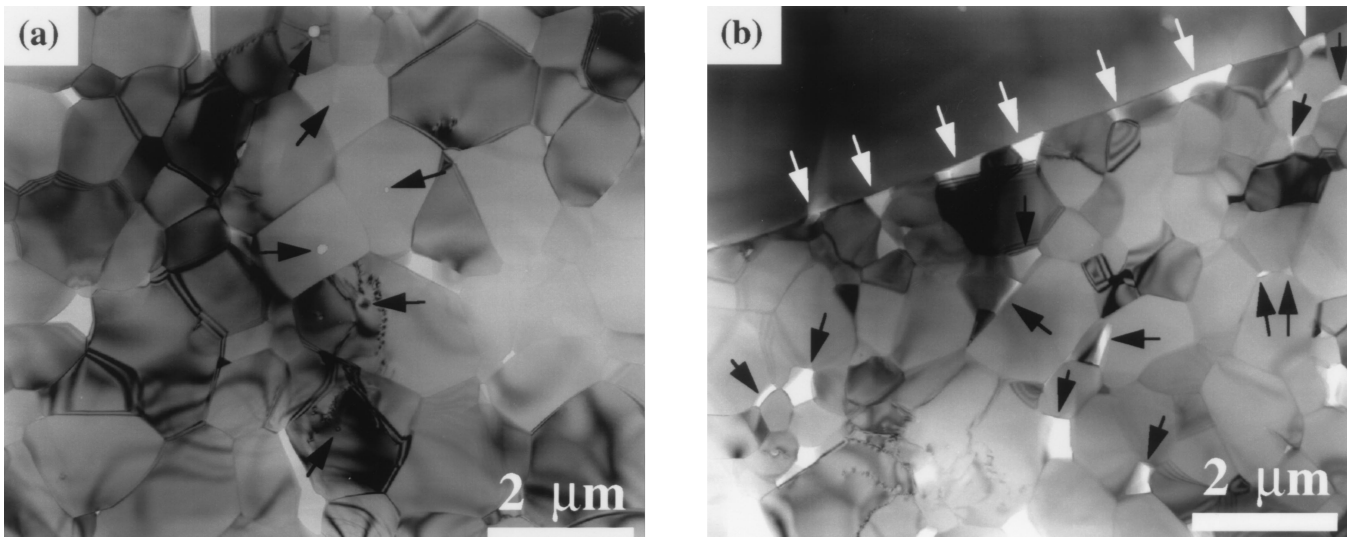

Fig. 3. TEM micrographs of the 350 ppm neodymium-doped material deformed at 1200°–1350°C and a stress of 50 MPa, for an accumulated strain of ~7%: (a) residual intragranular pores (indicated by arrows), (b) deformation-induced cavities within fine-grain-size regions (black arrows) and at the boundary between coarse and fine-grain-size clusters (white arrows).

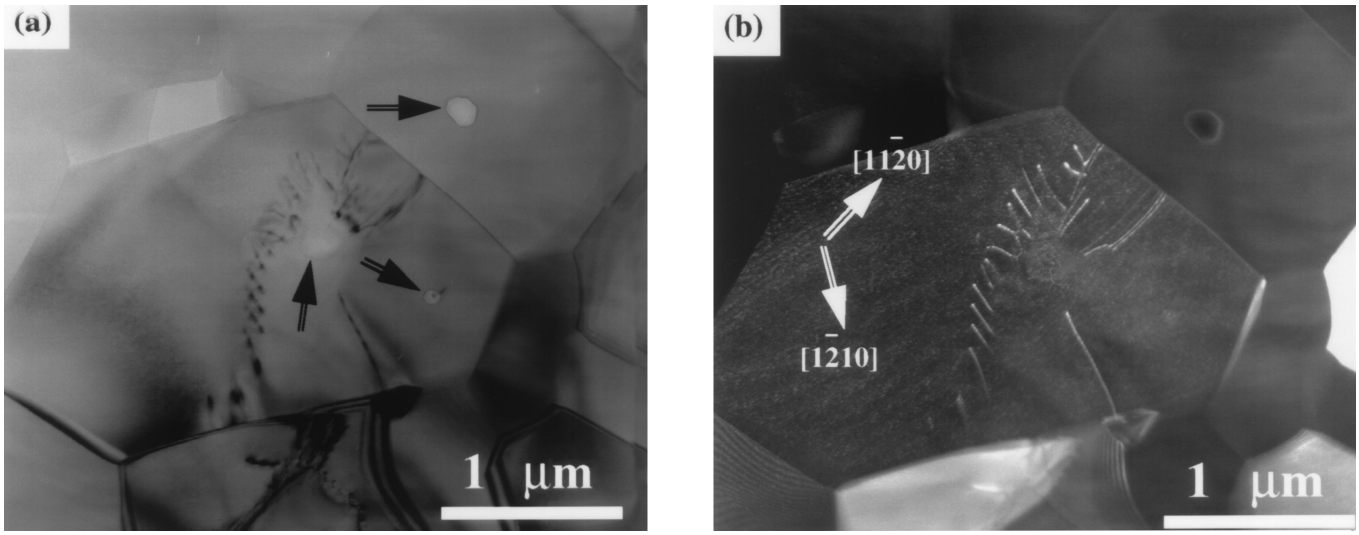

Fig. 4. TEM micrographs showing (a) faceting of the residual intragranular pores (indicated by arrows) and (b) dislocation arrays, which have a Burgers vector of $1/3\langle 11.0\rangle$.

The strain-rate data (at a constant tensile stress of 50 MPa) for the doped compositions are shown in Fig. 6; corresponding data for undoped Al_2O_3[4] are included, for reference. The apparent activation energy for tensile creep was derived from the slope of the curves and is plotted, as a function of dopant concentration, in Fig. 7. For comparison, values of the activation energy obtained by densification experiments on the same powder compositions are also plotted. (These latter experiments will be discussed in more detail in a separate paper.) Reasonable agreement exists between the two sets of data, and both sets suggest a trend whereby the activation energy first increases as the neodymium content increases and then saturates at a neodymium-dopant level of ~350–400 ppm.

The effect of the stress on the steady-state strain rate is shown in Fig. 8(a); the values of the stress exponent, *n*, were determined to be 2.1, 1.8, and 2.4 for the 100, 350, and 1000 ppm doped compositions, respectively. Hence, for the range of stress tested (20–75 MPa), the stress exponent is ~2 for all three dopant concentrations. This result is consistent with studies on other dopant systems obtained by the present group[2,4,7,15] and with work on undoped Al_2O_3 by Robertson *et al.*[8] As described earlier, the grain-size exponent, *p*, was determined by creep testing samples of different starting grain sizes at constant stress (50 MPa) and temperature (1275°C). Unfortunately, in the case of the 1000 ppm sample, annealing treatments did not provide a sufficient increase in the average grain size to enable the evaluation of *p*. However, for the 100 and 350 ppm doped samples, the values of *p* were 3.4 and 3.7, respectively (Fig. 8(b)).

In evaluating *p*, we used the average grain size, acquired by the linear-intercept method. In the 350 ppm neodymium-doped Al_2O_3 sample, some grains had a rather large grain size (>10 μm). Consequently, the validity of the linear-intercept method for obtaining the average grain size and, therefore, the grain-size exponent, *p*, is questionable in the present context. However, a compilation of the grain-size distributions for the 350 ppm neodymium-doped sample (Fig. 9) revealed that these outliers in the distribution comprise <3 vol% and are spatially isolated in the system. Thus, this small proportion of large grains is not expected to influence the strain rate of the material significantly. Detailed discussion of the effect of grain-size distribution on the creep strain rate will be discussed in a separate paper.

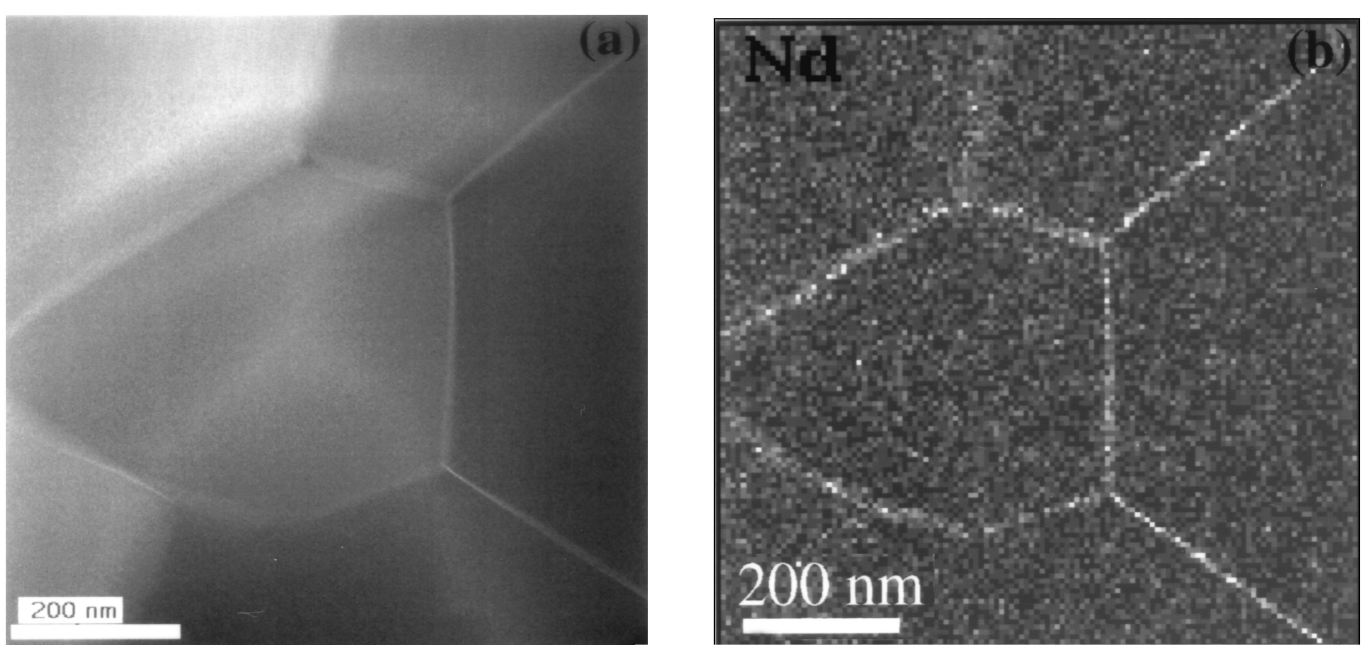

Fig. 5. (a) Annular-aperture dark-field STEM image and (b) energy-dispersive X-ray analysis map of neodymium distribution.

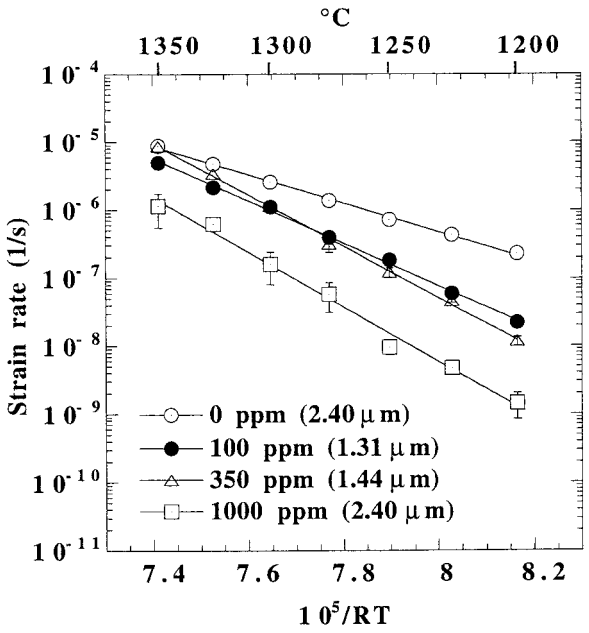

Fig. 6. Strain rate, as a function of temperature, for different neodymium dopant levels (50 MPa applied stress).

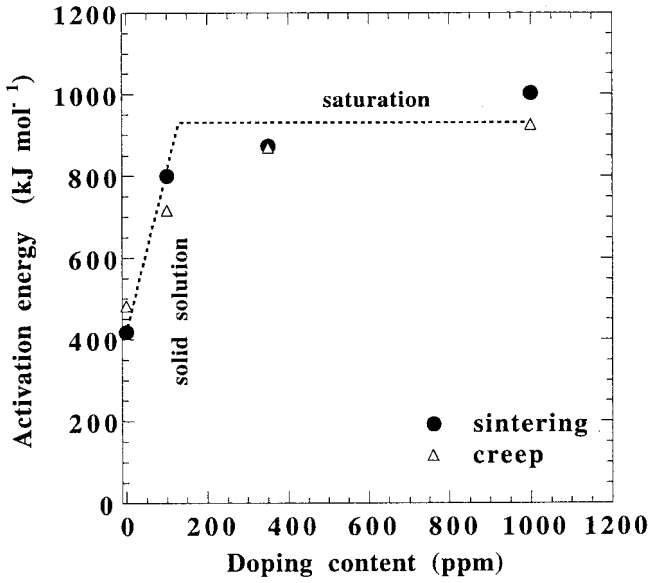

Fig. 7. Apparent activation energy (measured by both creep and sintering experiments), as a function of neodymium-doping content.

The effect of neodymium-dopant concentration on the creep behavior was evaluated by two distinct methods. Figure 10 shows the results of one of these approaches, in which creep data for the as-hot-pressed 100 and 350 ppm samples were corrected to the grain size of the 1000 ppm sample, using the *p* values determined previously. Under this approach, the creep data of the doped materials form a band that is distinct from that of the undoped Al_2O_3. Closer observation also reveals that the slope of the creep curves for the doped compositions reflect the difference in activation energy discussed earlier; hence, there is a crossover in the behavior at ~1275°C. Thus, depending on the creep temperature, the higher dopant level may be more or less beneficial, in terms of the strain rate.

In the second approach, the steady-state strain rate was compared for samples of different dopant compositions that had been annealed to achieve similar average grain sizes (2.4 ± 0.2 μm). Figure 11 shows that the degree of improvement in creep resistance is essentially independent of dopant composition. However,

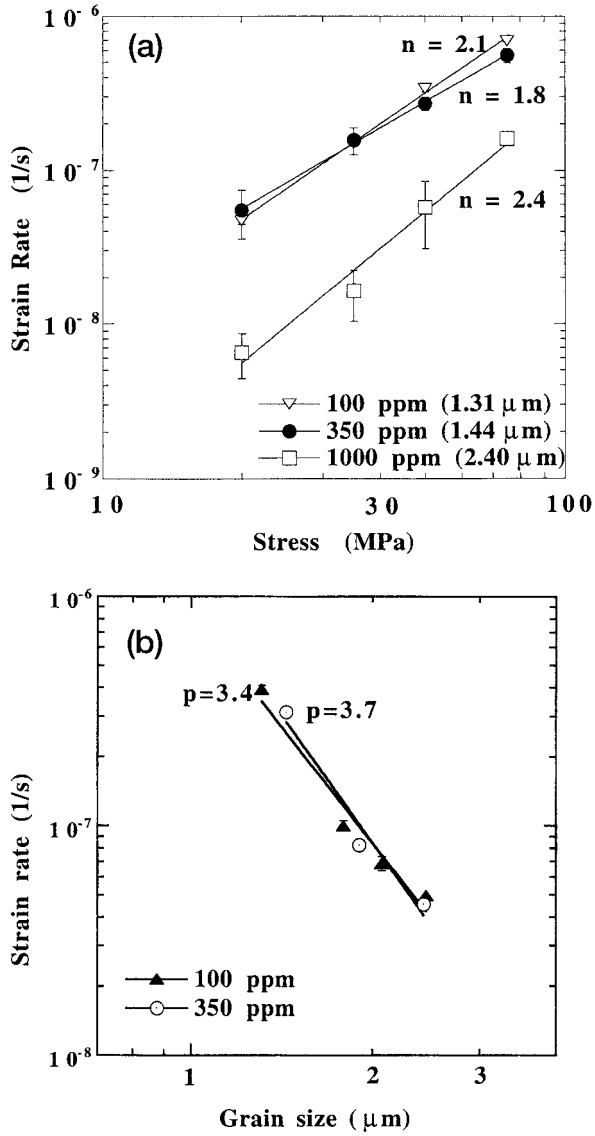

Fig. 8. Strain rate as a function of (a) stress (tested at 1275°C) and (b) grain size (50 MPa, 1275°C).

(coincidentally) the conditions tested (50 MPa, 1275°C) correspond to the region of the "crossover" of the strain-rate curves (see Fig. 10); hence, any dispersion in the strain rates is minimized. Nonetheless, the two sets of data are entirely consistent, and, taken as a whole, they show that the neodymium-dopant concentration (over the range 100–1000 ppm) does not have a strong effect on the degree of creep inhibition.

IV. Discussion

The present work demonstrates that singly doping Al_2O_3 with neodymium lowers the tensile creep rate by 2–3 orders of magnitude. Thus, the influence of neodymium is consistent with that of yttrium and lanthanum,[4] a result not altogether unexpected, given that the ionic radius of neodymium (0.98 Å) is intermediate between those of yttrium (0.90 Å) and lanthanum (1.03 Å). However, the present study was the first in which the neodymium-dopant concentration was systematically studied. The results show that the creep behavior, when normalized to account for grain size, is practically independent of the neodymium content. Because the dopant levels studied spanned the solubility limit, this finding confirms that the creep inhibition mechanism is primarily a solid-solution effect. The relative insensitivity of the creep behavior to dopant concentration is interesting and would seem to point

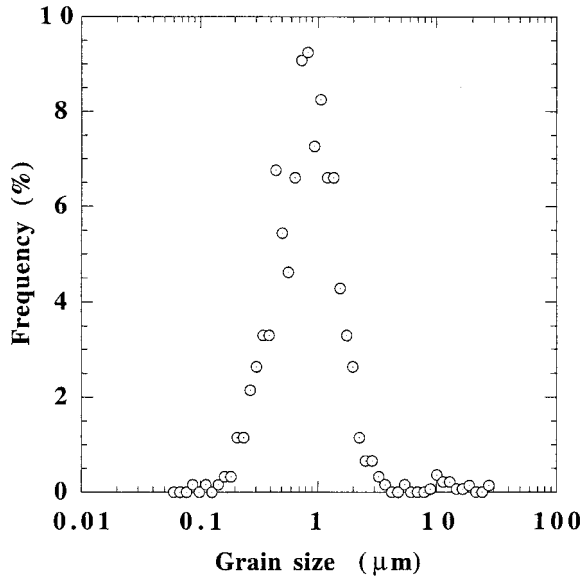

Fig. 9. Grain-size distribution of 350 ppm neodymium-doped Al_2O_3 (as-hot-pressed).

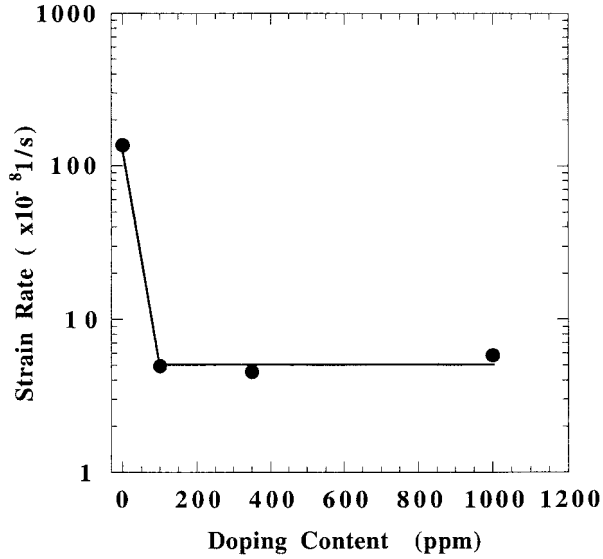

Fig. 11. Strain rate as a function of Nd_2O_3-doping level (50 MPa at 1275°C). All samples were preannealed to achieve a grain size of ~2.4 ± 0.2 μm.

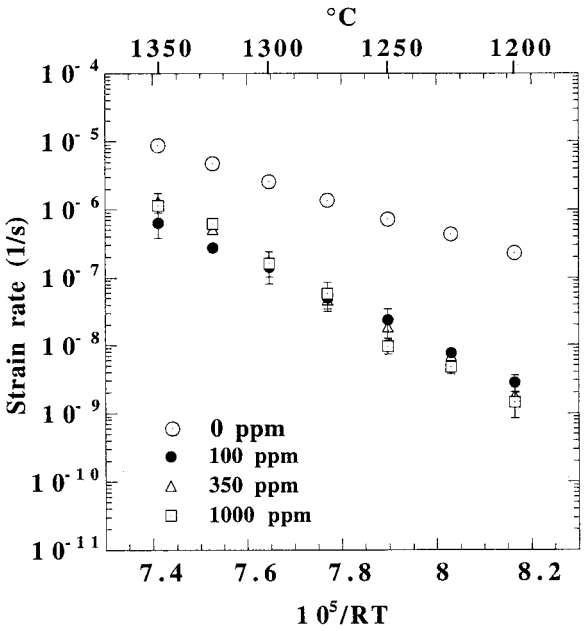

Fig. 10. Strain rate as a function of temperature (50 MPa applied stress). For all compositions, data were normalized to a grain size of 2.4 μm, according to the measured grain-size exponent.

to a saturation of Nd^{3+} ions at the grain boundary, and, hence, an upper limit to their effectiveness as obstacles to grain-boundary diffusion. However, the situation is more complex, because the present study also shows that the apparent activation energy (derived from both creep and densification experiments) increases as the dopant level increases.

One could speculate that the increase in the overall neodymium content correlates with an increase in the grain-boundary concentration and that interaction between the neodymium-occupied sites causes an initial increase in the activation energy. However, at the grain-boundary saturation level, no further increases would occur. Evidence to support this general picture is provided by ongoing AEM and extended X-ray absorption fine-structure studies,[16,17] which suggest that the local atomic environment of grain-boundary-segregated yttrium ions changes with yttrium concentration.

Similarly, in the Al_2O_3–ZrO_2 composite system, Wang and Raj[18] found that the apparent activation energy of Al_2O_3 during sintering increased initially as the ZrO_2 content increased (up to 5 vol% of ZrO_2), after which the apparent activation energy reached a saturation value. However, the trend of increasing activation energy with dopant level is in contrast to the results of Cho,[15] who reported that, in the case of lanthanum doping, the activation energies for 100 and 500 ppm samples were approximately the same (776 and 800 kJ/mol, respectively). However, for yttrium-doped Al_2O_3, Cho observed that the activation energy was lower for a 1000 ppm doped sample than for a 100 ppm sample (685 versus 832 kJ/mol). The reasons for this discrepancy are not well understood.

As proposed earlier, site-blocking of rapid grain-boundary diffusive paths seems to be the most logical explanation for the observed creep inhibition. The evidence supporting this mechanism (versus, for example, interface control) has been discussed in a previous work.[11] One compelling argument is that, for the range of grain sizes and stress and temperature conditions studied, grain-boundary diffusion is widely accepted as the rate-controlling step for Al_2O_3.[19] Furthermore, densification studies on doped aluminas have confirmed that grain-boundary diffusion is rate-controlling,[20] and the present study has shown that the values of the activation energy determined from creep and densification experiments are very comparable. Finally, orientation-image-mapping (OIM) studies do not reveal a significant difference between either the grain-boundary misorientation distribution or the proportion of coincident-site-lattice (CSL) boundaries in neodymium-doped Al_2O_3 versus undoped Al_2O_3.[21] This result rules out any possible role of the dopant ions in promoting particular boundaries with creep-resistant properties. However, the measured values of the grain size ($p \approx 3$–4) and stress exponent ($n \approx 2$), although once again consistent with previous results, cannot be reconciled with any generally accepted creep mechanism.[19,22–24]

In addition to its influence on the creep properties, the neodymium-dopant level also has a marked effect on the Al_2O_3 grain structure. The present study shows that neodymium concentrations in excess of the solubility limit result in an increased tendency for abnormal grain growth. This phenomenon is not processing-related, but rather a result of the effect of grain-boundary solute levels on the grain-boundary mobility. Recent STEM and grain-growth studies suggest that the onset of abnormal grain growth corresponds to a *supersaturation* of the solute at the Al_2O_3 grain boundary; these results are reported in a separate paper.[25]

V. Conclusions

Doping Al_2O_3 with 100 ppm Nd_2O_3 (which is below the solubility limit) reduces the tensile creep rate by 2–3 orders of magnitude. Dopant levels in excess of the solubility limit (350 and 1000 ppm) do not result in further substantial improvements in the creep, thus confirming that the beneficial influence of neodymium is primarily a solid-solution effect. The apparent creep activation energy increases with neodymium content and then saturates at ~950 kJ/mol for neodymium concentrations greater than the solubility limit. This trend is confirmed by activation energies derived from sintering experiments. The increase in activation energy (relative to that of undoped Al_2O_3) is probably attributable to site-blocking by the oversized Nd^{3+} ions, which segregate to the Al_2O_3 grain boundaries. It is tentatively suggested that the saturation in the activation energy subsequent to increasing the neodymium concentration corresponds to a greater likelihood of interaction between adjacent neodymium-occupied sites.

Given that the present grain structures were markedly less homogeneous in the case of the 350 and 1000 ppm dopant concentrations, the saturation in the creep benefit suggests an optimum dopant level at which the grain-boundary dopant concentration just exceeds the solubility limit. The results of the present study are completely consistent with creep studies conducted on other rare-earth dopant systems (yttrium and lanthanum) and, once more, suggest a site-blocking mechanism whereby the oversized dopant ions impede grain-boundary diffusion.

Acknowledgments

The authors are grateful to R. Krause, National Institute of Standards and Technology, for his assistance with hot-pressing of the materials and for helpful suggestions regarding improved accuracy in acquiring the creep data. We also wish to thank G. Thompson for assistance in determining the grain-size distribution and J. M. Chabala, K. L. Gavrilov, and R. Levi-Setti, University of Chicago, for conducting the SIMS characterizations. This work was monitored by Dr. A. Pechenik.

References

[1]S. Lartigue, C. Carry, and L. Priester, "Grain Boundaries in High Temperature Deformation of Yttria and Magnesia Co-Doped Alumina," *J. Phys. (Paris)*, **C1–51**, 985–90 (1990).

[2]J. D. French, J. Zhao, M. P. Harmer, H. M. Chan, and G. A. Miller, "Creep of Duplex Microstructure," *J. Am. Ceram. Soc.*, **77**, 2857–65 (1994).

[3]S. Korinek and F. Dupau, "Grain Boundary Behavior in Superplastic Mg-Doped Alumina with Yttria Co-doping," *Acta Metall. Mater.*, **42**, 293–302 (1994).

[4]J. Cho, M. P. Harmer, H. M. Chan, J. M. Rickman, and A. M. Thompson, "Effect of Yttrium and Lanthanum on the Tensile Creep Behavior of Aluminum Oxide," *J. Am. Ceram. Soc.*, **80**, 1013–17 (1997).

[5]A. M. Thompson, H. M. Chan, and M. P. Harmer, "Tensile Creep of Alumina–Silicon Carbide Nanocomposites," *J. Am. Ceram. Soc.*, **80**, 2221–28 (1997).

[6]A. M. Thompson, K. K. Soni, H. M. Chan, M. P. Harmer, D. B. Williams, J. M. Chabala, and R. L. Setti, "Dopant Distribution in Rare-Earth-Doped Alumina," *J. Am. Ceram. Soc.*, **80**, 373–76 (1997).

[7]Y. Z. Li, C. M. Wang, H. M. Chan, J. M. Rickman, M. P. Harmer, J. M. Chabala, K. L. Gavrilov, and R. Levi-Setti, "Codoping of Alumina to Enhance Creep," *J. Am. Ceram. Soc.*, **82**, 1497–504 (1999).

[8]A. J. Robertson, D. S. Wilkinson, and C. H. Caceres, "Creep and Creep Fracture in Hot-Pressed Alumina," *J. Am. Ceram. Soc.*, **74**, 915–20 (1991).

[9]F. Wakai, T. Nagano, and T. Iga, "Hardening in Creep of Alumina by Zirconium Segregation at the Grain Boundary," *J. Am. Ceram. Soc.*, **80**, 2361–66 (1997).

[10]F. Wakai, T. Iga, and T. Nagano, "Effect of Dispersion of ZrO_2 Particles on Creep of Fine-Grained Alumina," *J. Ceram. Soc. Jpn.*, **96**, 1206–209 (1988).

[11]J. Cho, C. M. Wang, H. M. Chan, M. P. Harmer, and J. M. Rickman, "Role of Segregation Dopants on the Improved Creep Resistance of Aluminum Oxide," *Acta Mater.*, **47**, 4197–207 (1999).

[12]J. D. French and S. M. Wiederhorn, "Tensile Specimens from Ceramic Components," *J. Am. Ceram. Soc.*, **79**, 550–52 (1996).

[13]A. H. Chokshi and J. R. Porter, "Cavity Development during Creep Deformation in Alumina with a Bimodal Grain Size Distribution," *J. Am. Ceram. Soc.*, **70**, 197–202 (1987).

[14]B. J. Dalgleish, S. M. Johnson, and A. G. Evans, "High-Temperature Failure of Polycrystalline Alumina: I, Crack Nucleation," *J. Am. Ceram. Soc.*, **67**, 741–50 (1984).

[15]J. Cho, "Role of Rare-Earth Dopant on the Improved Creep Properties of Aluminum Oxide"; Ph.D. Thesis. Lehigh University, Bethlehem, PA, 1998.

[16]C. M. Wang, G. S. Cargill III, M. P. Harmer, H. M. Chan, and J. Cho, "Atomic Structural Environment around Grain Boundary Segregated Y and Zr in Creep Resistant Alumina," *Acta Mater.*, **47**, 3411–22 (1999).

[17]C. M. Wang, G. S. Cargill III, H. M. Chan, and M. P. Harmer, "Structural Features of Y-Saturated and Supersaturated Grain Boundaries in Alumina," *Acta Mater.*, **48**, 2579–91 (2000).

[18]J. Wang and R. Raj, "Activation Energy for the Sintering of Two-Phase Alumina/Zirconia Ceramics," *J. Am. Ceram. Soc.*, **74**, 1959–63 (1991).

[19]R. M. Cannon and R. L. Coble, "Review of Diffusional Creep of Al_2O_3"; pp. 61–100 in *Deformation of Ceramic Materials*. Edited by R. C. Bradt and R. E. Tressler. Plenum Press, New York, 1975.

[20]J. Fang, A. M. Thompson, M. P. Harmer, and H. M. Chan, "Effect of Yttrium and Lanthanum on the Sintering Behavior of Ultra-High-Purity Al_2O_3," *J. Am. Ceram. Soc.*, **80**, 2005–12 (1997).

[21]J. Cho, C. M. Wang, H. M. Chan, M. P. Harmer, and J. M. Rickman, "A Study of Grain Boundary Structure in Rare-Earth-Doped Alumina Using the EBKD Technique," submitted to *J. Mater. Sci*.

[22]P. A. Lessing and R. S. Gordon, "Creep of Polycrystalline Alumina, Pure and Doped with Transition Metal Impurities," *J. Mater. Sci.*, **12**, 2291–302 (1977).

[23]F. R. N. Nabarro, "Deformation of Crystals by Motion of Single Ions"; p. 231 in *Report of a Conference on the Strength of Solids*. Physical Society, London, U.K., 1948.

[24]C. Herring, "Diffusional Viscosity of a Polycrystalline Solid," *J. Appl. Phys.*, **21**, 437–41 (1950).

[25]C. M. Wang, H. M. Chan, M. P. Harmer, and J. M. Rickman; unpublished research. □